Chemical Engineering Journal 545 (2026) 179238

Contents lists available at ScienceDirect

Chemical Engineering Journal

journal homepage: www.elsevier.com/locate/cej

Carbon fabrics for electrified direct air capture: From substrate morphology to module-scale operating trade-offs

Carla Esch [a], Jacqueline Kieven [a], Antonia Geiser [a], Roman Ryapushkin [a], Wibke Zängler [a], Matthias Wessling [a,b,*]

[a] Chemical Process Engineering AVT.CVT, RWTH Aachen University, Forckenbeckstraße 51, 52074 Aachen, Germany
[b] DWI – Leibniz-Institute for Interactive Materials, Forckenbeckstraße 50, 52074 Aachen, Germany

ARTICLE INFO

Keywords:
Direct air capture
Electrified temperature swing adsorption
Carbon fabric
Polyethyleneimine
Sorbent morphology
Spiral wound module

ABSTRACT

Polyethyleneimine (PEI)-impregnated carbon fabrics are structured direct air capture (DAC) sorbents whose electrical conductivity enables resistive temperature swing regeneration. However, how substrate morphology translates intrinsic sorbent properties into module-scale DAC performance under continuous flow remains poorly understood. We investigate this using a resistively heated spiral wound module (SWM). Two carbon fabrics, a macroporous non-woven (E20) and a microporous activated carbon cloth (FM10), were characterized. Thermogravimetric analysis revealed a trade-off between CO_2 capacity and kinetics: higher PEI loading enhanced capacity but slowed sorption and desorption. FM10 showed faster kinetics than E20, yet its higher surface area did not increase CO_2 uptake, indicating that accessibility rather than amine content governed the usable capacity. The kinetically favorable FM10 was deployed in the SWM under DAC-relevant conditions (400 ppm CO_2). Comparison of intrinsic and dynamic performance revealed that only 15-30 % of the intrinsic capacity was utilized under continuous-flow operation, demonstrating that DAC performance is governed by transport limitations rather than equilibrium sorbent properties alone. Reducing gas flow rate improved dynamic yield at the expense of productivity. Humid operation enhanced yield through water-induced PEI swelling while reducing the specific regeneration energy. This energy was dominated by parasitic heat loss rather than by the sorbent, identifying module heat management, alongside dynamic utilization, as a design-limited lever. These results show that the dominant challenge in electrified DAC is not maximizing intrinsic sorbent capacity, but maximizing its dynamic utilization through the coupled design of substrate morphology, PEI distribution, module architecture, and operating strategy.

1. Introduction

Rising anthropogenic carbon dioxide (CO_2) concentrations in the atmosphere drive climate change, demanding effective negative emission technologies to counteract global warming. In addition to point sources, a substantial share of annual CO_2 emissions originates from distributed sources such as buildings and households [1,2]. Direct air carbon capture and storage (DACCS) enables compensation of distributed emissions and removal of historical atmospheric CO_2 by separating CO_2 directly from ambient air for subsequent permanent storage.

Among the separation concepts demonstrated in pilot and commercial direct air capture (DAC) plants, liquid-solvent absorption using aqueous potassium carbonate or amino-acid solutions and solid-sorbent vacuum temperature swing adsorption (VTSA) represent the most mature routes [3–5]. In VTSA, CO_2 is captured at ambient conditions and released at elevated concentration through the combined application of heating and vacuum. Commercial systems commonly employ amine-functionalized solid sorbents that regenerate below 100 °C [6]. However, regeneration relies on indirect heat transfer via heated purge gas or steam, which increases thermal energy demand and can dilute the product stream, requiring downstream separation [7]. In addition, the dependence on external heat infrastructure limits flexibility for decentralized applications. These constraints motivate regeneration strategies that enable direct and locally available heat delivery.

Electrified temperature swing operation offers a route toward directly coupled heat generation within the sorbent structure using only electricity. Among electrified heating approaches, resistive (Joule) heating is a promising approach owing to its simplicity and its potential for rapid heating when the substrate is electrically conductive. Achieving uniform temperature distribution across a contactor remains

* Correspondence to: Forckenbeckstraße 51, 52074 Aachen, Germany.
E-mail address: manuscripts.cvt@avt.rwth-aachen.de (M. Wessling).

https://doi.org/10.1016/j.cej.2026.179238
Received 13 May 2026; Received in revised form 18 June 2026; Accepted 7 July 2026
Available online 13 July 2026
1385-8947/© 2026 The Authors. Published by Elsevier B.V. This is an open access article under the CC BY license (http://creativecommons.org/licenses/by/4.0/).

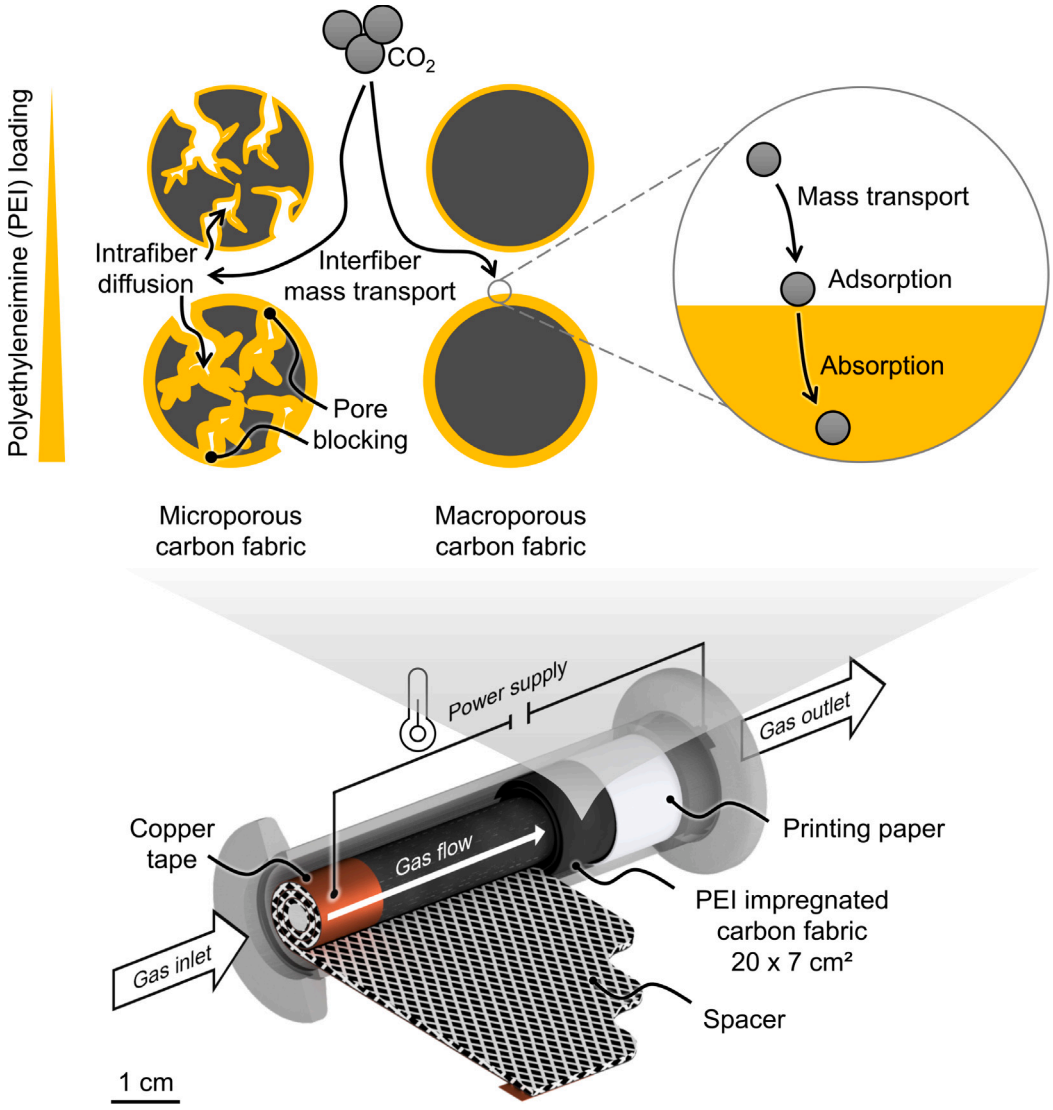


Fig. 1. Parameters governing the performance of sorbent-impregnated carbon fabrics for direct air capture in a spiral wound module: substrate porosity, homogeneity and thickness of the PEI coating, inter- and intrafiber mass transport, combined adsorption and absorption, regeneration strategy, module design, and process parameters.

an important design consideration, however, as local hot spots can arise depending on the current pathway and contact geometry [8]. Carbon-based monoliths, fibers, and fabrics are therefore attractive structured supports for DAC sorbents because they host the functional sorbent while their intrinsic electrical conductivity additionally enables resistive heating within the sorbent matrix [9–17].

In structured adsorption systems operated under DAC-relevant conditions, dynamic CO_2 loading can remain below the intrinsic sorbent capacity measured under equilibrium or gravimetric conditions [15,18,19]. This intrinsic-to-dynamic utilization gap reflects the combined influence of diffusion limitations, gas–solid mass transfer, and finite residence times inherent to continuous-flow operation. In electrically regenerated contactors based on polyethyleneimine (PEI)-impregnated carbon fabrics, these transport effects are strongly coupled to the effective morphology of the sorbent layer. CO_2 uptake in PEI involves a rapid interfacial reaction followed by slower diffusion into the polymer bulk, making the usable capacity sensitive to polymer distribution, effective coating thickness, and environmental humidity [20–22]. In such systems, substrate morphology acts as a mediator between sorbent loading and dynamic performance: the pore and void structure of the carbon substrate influences the spatial distribution, thickness, and accessibility of the deposited PEI, thereby affecting transport pathways during dynamic operation. This interplay between substrate porosity, coating architecture, and intra- and interfiber transport is schematically illustrated in Fig. 1.

Accordingly, how substrate morphology and PEI distribution govern the intrinsic-to-dynamic utilization gap, and how this couples to operating parameters, remains insufficiently resolved for electrically regenerated DAC contactors. Although structure–property relationships have been investigated for alternative functionalizations, such as hydroxide-functionalized carbon cloths [23], systematic linkage between substrate morphology, PEI coating architecture, and dynamic module-scale performance remains insufficiently resolved.

In this work, we provide an integrated study of PEI-impregnated carbon fabrics as electrically heatable, structured DAC sorbents on a resistively heated contactor platform. Our prior work introduced the resistively heated spiral wound module (SWM) concept [17]. Here, resistive heating is considered an enabling feature of the conductive substrate rather than the primary object of investigation. We address ambient DAC conditions at 400 ppm CO_2, including humidity, and compare two structurally distinct fabrics, the macroporous E20 and the microporous FM10. The guiding question is what governs the usable

Table 1
Characteristics of the carbon fabrics E20 and FM10.

Fabric	Fiber orientation	Thickness (μm)	Surface density ($g\,m^{-2}$)	Surface area ($m^2\,g^{-1}$)
E20	Non-woven	210	95	5.80
FM10	Plain woven	500	120	1012 ± 23

fraction of the intrinsic capacity under continuous flow: the material itself, or the coupled design of substrate morphology, PEI loading, and module operation.

We (i) establish that both fabrics provide electrically heatable supports and compare their heating homogeneity, (ii) quantify how substrate structure influences PEI uptake and coating morphology and how this translates into intrinsic CO_2 capacity and kinetics, (iii) evaluate dynamic breakthrough performance in a compact SWM under DAC-relevant conditions by controlled variation of PEI loading, gas flow rate, and humidity, and (iv) translate these findings into process-relevant performance metrics and module-design implications. Together, these experiments reveal how substrate architecture, PEI distribution, and operating conditions determine the transition from intrinsic sorbent properties to module-scale DAC performance. In doing so, we revisit the hypothesis from our previous work [17] that substrates enabling thin and accessible PEI coatings are the primary route toward reducing the intrinsic-to-dynamic utilization gap.

2. Experimental

Two electrically conductive carbon fabrics with distinct structural characteristics were investigated as substrates for electrically regenerated CO_2 sorbents. Their electrothermal response, intrinsic CO_2 sorption behavior after amine functionalization, and dynamic performance in a resistively heated SWM were systematically evaluated. Dynamic breakthrough experiments of one fabric were conducted under DAC-relevant conditions while varying PEI loading, gas flow rate, and humidity.

2.1. Carbon fabrics

Two commercially available carbon fabrics were selected as electrically conductive supports: E20 (Freudenberg Performance Materials), a non-woven macroporous carbon paper, and Flexzorb FM10 (Long Life for Art), a woven microporous activated carbon cloth. The manufacturer-reported properties and the specific Brunauer–Emmett–Teller (BET) surface areas determined by nitrogen (N_2) physisorption are summarized in Table 1. Detailed BET measurement conditions are provided in Section 2 in the Supplementary Information (SI).

2.2. Electrothermal characterization

For electrothermal characterization, 4×4 cm^2 samples were electrically contacted by attaching 6 mm wide copper tape (3M) to two opposing edges on both the front and back sides of the fabric. The contacts were pressed at $1000\,kN\,m^{-2}$ for 1 min at room temperature using a hot press (Polystat 300 S/2, Buehler) to ensure uniform and reproducible electrical contact. The samples were connected to DC power supplies and operated at constant current. E20 samples were tested between 2-3 A (N5762A, Keysight Technologies), whereas FM10 samples were tested between 0.15-0.37 A (HM8143, Rohde & Schwarz), with current ranges selected to achieve comparable specific power levels across both fabrics. The electrical power was calculated as $P = U \cdot I$, where U denotes the applied voltage and I the current, and the specific power was defined as the applied electrical power normalized to the projected sample area between the electrodes. Surface temperature was measured using two type K thermocouples (Therma), electrically insulated with Kapton tape (a polyimide film that prevents a short circuit through the conductive substrate without measurably affecting the temperature reading, given its negligible thermal resistance at the thicknesses used) and attached to the fabric surface. The thermocouples were positioned centrally between the electrical contacts and laterally separated across the fabric width to assess temperature homogeneity (see Figure S1 in the SI). Each sample was heated for 1000 s, followed by passive cooling under ambient conditions. Heating and cooling rates were determined from the initial 10 s of the respective temperature profiles.

2.3. Impregnation of the carbon fabrics

The carbon fabrics were functionalized by dip coating using PEI (800 Da, Sigma-Aldrich) dissolved in ethanol (99.8 %, Supelco). Coating solutions containing 5, 10, 20 and 30 wt.% PEI were prepared and used without further modification. For impregnation, the fabrics were vertically mounted in a custom-built dip-coating device and immersed into the coating solution at a controlled speed of $4.65\,mm\,s^{-1}$. After a dwell time of 10-20 s, the samples were withdrawn at the same speed. Each fabric was coated once. Following impregnation, the samples were dried in a vacuum oven (VO101, Memmert) at 30 °C and 75 mbar for at least 24 h. The PEI loading was determined gravimetrically from the mass difference before and after coating. Impregnated samples are denoted as *FABRIC-PEIX-Y*, where *FABRIC* refers to E20 or FM10, *X* indicates the PEI concentration in the coating solution (wt.%), and *Y* denotes the dwell time (s).

2.4. Sorbent characterization

The morphology of the pristine and PEI-functionalized fabrics was analyzed by scanning electron microscopy (SEM, FESEM SU5000, Hitachi). Before imaging, the samples were sputter-coated with a gold/palladium layer (80/20) using a sputter coater (Q300TT, Quorum Technologies) to ensure electrical conductivity.

Intrinsic CO_2 sorption capacity and kinetics were evaluated using thermogravimetric analysis (TGA, STA6000, PerkinElmer). Samples were initially degassed at 120 °C for 80 min under a flow of $150\,mL\,min^{-1}$ N_2. Then, the flow rate was adjusted to $50\,mL\,min^{-1}$ and the sample was cooled to 30 °C. Sorption was conducted using 400 ppm CO_2 in argon for 120 min. Regeneration was initiated by heating to 120 °C while maintaining the same gas composition and flow rate. Desorption was recorded for 15 min. The CO_2 loading was calculated from the recorded mass change. Sorption and desorption kinetics were analyzed using the Avrami kinetic model [24]. Identical measurements were performed using the commercial primary-amine-functionalized ion-exchange resin Lewatit VP OC 1065 (Sigma-Aldrich) as a benchmark material.

2.5. Spiral wound module assembly

The SWM was based on our previously reported resistively heated design [17]. Only adaptations from the earlier configuration are described here. To increase the volumetric packing density of the spiral, the spacer design was modified. Instead of expanded polytetrafluoroethylene (PTFE) spacer strips (thickness 1 mm), polyester mesh spacers (PET0277/60, PVF Mesh & Screen Technology) with a thickness of 134 μm were inserted between adjacent windings. The reduced spacer thickness enabled a higher number of windings within the same housing volume. Accordingly, woven activated carbon fabric (FM10) sheets measuring 20×7 cm^2 were used, extending the sheet length in the winding direction while maintaining the module length. For improved

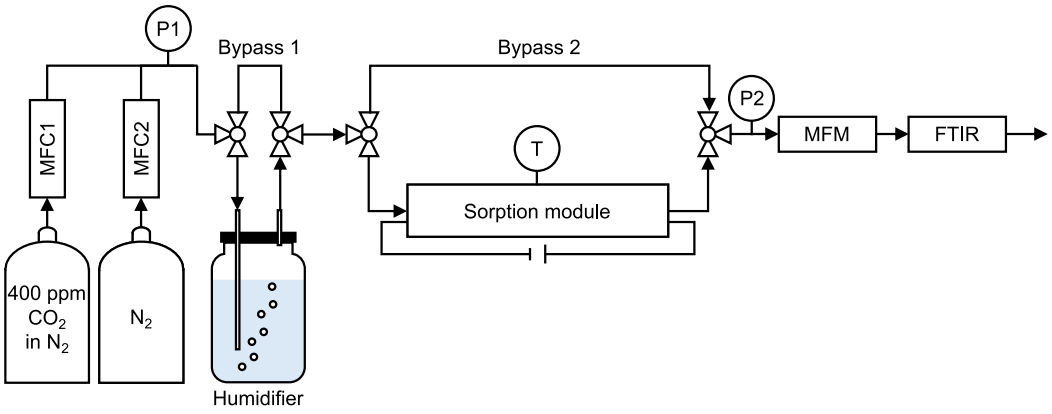


Fig. 2. Flow sheet of the breakthrough curve setup used to perform resistively heated temperature swings of the spiral wound module.

handling during assembly, the PTFE support tube length was increased to 8 cm (outer diameter 4 mm). The internal volume of the assembled module is approximately 14 cm^3. A schematic of the module assembly is provided in Figure S7 in the SI. All other assembly steps, electrical contacting, instrumentation, and housing configuration are described in our previous work [17].

2.6. Dynamic breakthrough experiments

Dynamic CO_2 sorption and regeneration experiments were performed using a custom breakthrough setup enabling controlled gas composition, humidity conditioning, and resistive heating of the spiral wound module.

As illustrated in Fig. 2, the feed gas was supplied from a gas bottle containing 400 ppm CO_2 in N_2 (Westfalen), while N_2 was used as sweep and regeneration gas. Nitrogen was used as the carrier and sweep gas to isolate CO_2 sorption and transport behavior under a controlled composition. Ambient air additionally contains oxygen, which can cause oxidative degradation of the amine over extended operation [25]. This effect is not captured by the inert-gas experiments here and would need to be assessed under realistic feed conditions. Gas flow rates were regulated using mass flow controllers (MFC, MC 0-100 sccm, Alicat Scientific). The inlet stream was either directed to the module or through a humidifier to establish humidified conditions. Both the humidifier and the module were equipped with bypass lines to enable controlled switching between dry and humid operation without interrupting the gas supply. The module temperature was manually controlled via resistive heating using a DC power supply (HM8143, Rohde & Schwarz Hameg) with feedback from integrated type K thermocouples. Outlet CO_2 and H_2O concentrations were measured continuously using a Fourier-transform infrared spectroscopy (FTIR) gas analyzer (CX4000, Gasmet Technologies). The outlet flow rate was monitored using a mass flow meter (MFM, M 0-100 sccm, Alicat Scientific), and the pressure drop across the module was recorded using pressure sensors (P-30, 0-4 bar, WIKA). All signals were logged via NI LabVIEW.

Prior to each experiment, the module was regenerated at 120 °C under 100 sccm N_2 to remove residual CO_2 and moisture. After cooling to ambient temperature under continued N_2 flow, sorption was initiated by switching the inlet gas to 400 ppm CO_2 in N_2 at the specified flow rate. For humid experiments, the module was first presaturated with humidified N_2 until the outlet H_2O concentration reached steady state. Then, the humidifier was equilibrated with 400 ppm CO_2 while bypassing the module to ensure a stable inlet composition. Subsequently, the humidified CO_2/N_2 mixture was directed through the module to initiate sorption. Regeneration was conducted by resistive heating to approximately 110-120 °C under dry N_2 flow.

The dynamic CO_2 loading q was calculated from the outlet concentration profiles and normalized to the total mass of carbon fabric and PEI according to Eq. (1):

$$q = \frac{\dot{V}_{\mathrm{MFC}} \cdot c_{0,\mathrm{CO_2}}}{V_{\mathrm{m}} \cdot m_{\mathrm{CF+PEI}}} \int_0^t \left(1 - \frac{c_{\mathrm{CO_2}}}{c_{0,\mathrm{CO_2}}}\right) \mathrm{d}t \tag{1}$$

where $\dot{V}_{\mathrm{MFC}}$ is the inlet volumetric flow rate, $c_{0,\mathrm{CO_2}}$ and $c_{\mathrm{CO_2}}$ denote inlet and outlet CO_2 concentrations, V_{m} is the molar gas volume at the standard reference conditions of the mass flow controller, 25 °C and 1.013 bar, and $m_{\mathrm{CF+PEI}}$ is the mass of the impregnated carbon fabric. The dynamic loading was baseline-corrected. Corrections for the outlet flow rate, the pressure drop, the inlet humidity, and the module dead volume were not applied, as their contributions to the integral are negligible under the conditions used here.

In addition to dynamic CO_2 loading, three process-oriented performance indicators were used to compare experiments within this study:

- Dynamic yield: The fraction of the fed CO_2 captured up to breakthrough, expressed in percent and obtained from the outlet concentration profile.
- Product concentration: The peak outlet CO_2 concentration during regeneration, reported on a wet basis and including dilution by the N_2 sweep gas.
- Productivity: Amount of captured CO_2 per unit time, normalized either to the sorbent mass or to the internal module volume.

To enable consistent comparison of dynamic yield across experimental series, breakthrough was defined at a relative outlet concentration of $c_{\mathrm{CO_2}}/c_{0,\mathrm{CO_2}} = 0.1$, corresponding to 40 ppm CO_2 at the applied inlet concentration of 400 ppm.

Dynamic breakthrough experiments were performed to investigate the influence of (i) PEI loading, (ii) gas flow rate, (iii) humidity, and (iv) cyclic stability. The duration of the sorption step was set by the objective of the respective series, and switching from sorption to regeneration was performed manually, which introduced some variation in the exact endpoint. For PEI loading comparisons, sorption was continued until the outlet concentration exceeded 300 ppm. For flow-rate variation experiments, sorption was evaluated up to a dynamic loading of 0.3 mmol g^{-1}. For humidity and cyclic stability experiments, sorption was continued for up to 8 h followed by 4 h of desorption. Comparisons within each experimental series were performed under identical stopping criteria. An overview of all dynamic breakthrough experiments, their conditions, and stopping criteria is provided in Table 2. The criterion was chosen to suit the objective of each series, so the resulting indicators are comparable within a series but not directly across series.

Table 2
Overview of the dynamic breakthrough experiments, the parameter varied in each series, and the corresponding stopping criterion.

Series	Sorbent	Flow (sccm)	Humidity	Stopping criterion
PEI loading	FM10-PEI5-20, FM10-PEI30-10	100	dry	outlet > 300 ppm
Flow rate	FM10-PEI30-10	50, 100	dry	loading 0.3 mmol g^{-1}
Humidity	FM10-PEI30-10	50	dry, humid	up to 8 h
Cyclic stability	FM10-PEI30-10	100	dry	8 h sorption, 4 cycles

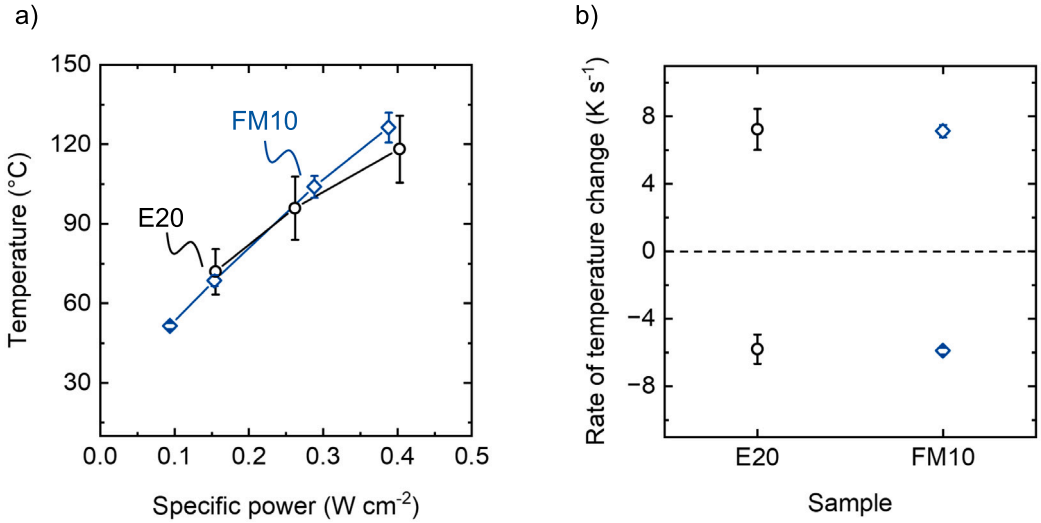


Fig. 3. Resistive heating behavior of 4 × 4 cm^2 samples of the carbon fabrics E20 and FM10. The standard deviation results from the temperature distribution measured with two thermocouples in the same experiment. (a) Maximum temperature as a function of applied specific power. (b) Heating and cooling rates were determined from the first 10 s of heating to 120 °C and cooling to room temperature.

3. Results and discussion

3.1. Resistive heating

The resistive heating performance of FM10 was evaluated and compared to the previously characterized E20 [17] to assess its suitability as an electrically conductive support for rapid temperature swing operation. Fig. 3a summarizes the steady-state surface temperature as a function of applied specific power, while Fig. 3b shows the corresponding heating and cooling rates derived from the initial 10 s of the temperature transients.

For both fabrics, the steady-state temperature increased approximately linearly with increasing specific power, indicating stable ohmic heating. The same specific power was achieved at different operating currents for the two fabrics (2-3 A for E20 versus 0.15-0.37 A for FM10, see Section 2.2), reflecting their distinct intrinsic resistivities (see Figure S2 in the SI). At a specific power of 0.4 W cm^{-2}, FM10 reached surface temperatures of 120-125 °C, matching the previously reported response of E20 [17] and confirming its suitability for resistive regeneration at module scale. The transient response was similarly fast for both fabrics, with heating and cooling rates of approximately 7 K s^{-1} and 6 K s^{-1}, respectively.

Despite comparable mean temperatures and kinetics, FM10 exhibited a smaller temperature deviation between the two thermocouples than E20, indicating improved lateral temperature homogeneity. This difference is attributed to the woven architecture of FM10 (see Fig. 4), which provides continuous and spatially uniform current pathways. In contrast, the non-woven structure of E20 results in locally varying fiber contacts and current densities, leading to enhanced spatial temperature gradients. Overall, both substrates are therefore electrically suitable for the module application.

3.2. PEI loading and sorbent morphology

To introduce selective CO_2 uptake, the carbon fabrics were impregnated with PEI. The influence of coating conditions on polymer uptake and resulting morphology was evaluated gravimetrically and by SEM. Table 3 quantifies the PEI loading depending on the solution concentration and dwell time, while Fig. 4 illustrates the corresponding morphological changes.

For both fabrics, the PEI loading increased monotonically with increasing solution concentration. Under identical coating conditions, FM10 consistently achieved higher PEI loadings than E20 and exhibited a larger standard deviation. Extending the dwell time from 10 s to 20 s for FM10-PEI5 further increased polymer uptake, indicating that impregnation kinetics and pore accessibility contribute to the final loading.

The higher loadings obtained for FM10 are consistent with its larger specific surface area, which facilitates polymer retention and capillary-driven uptake. The increased variability in loading observed for FM10 likely reflects surface heterogeneities and local differences in wettability that affect polymer distribution during dip coating.

SEM analysis reveals distinct coating morphologies for the two substrates. For E20, low PEI concentrations produced thin and relatively uniform fiber coatings, whereas higher concentrations led to partial filling of interfiber voids and increased fiber-to-fiber bridging. In contrast, the initially rough surface of FM10 was progressively smoothened upon impregnation, particularly at higher PEI loadings, indicating pore filling of the activated carbon texture.

Taken together, the gravimetric and microscopic observations demonstrate that substrate structure strongly influences polymer distribution. While FM10 accommodates higher polymer amounts due to its high surface area and microporous texture, increasing PEI loading in both fabrics promotes pore filling and thickening of the polymer phase, which is expected to influence amine accessibility and internal mass transport during subsequent CO_2 sorption.

3.3. CO_2 sorption capacity and kinetics

TGA was employed to determine the intrinsic CO_2 sorption capacity and sorption/desorption kinetics of the PEI-impregnated fabrics under

Table 3
PEI loading of E20 and FM10 carbon fabrics (CF) after 5, 10, 20 and 30 wt.% PEI impregnation. All impregnations used a dwell time of 10 s. FM10 impregnated with 5 wt.% PEI was additionally tested with a dwell time of 20 s.

Impregnation	PEI loading of FM10 ($g_{PEI}\ g_{CF}^{-1}$)	PEI loading of E20 ($g_{PEI}\ g_{CF}^{-1}$)
PEI5-10	0.10 ± 0.03	0.09 ± 0.02
PEI5-20	0.12 ± 0.05	
PEI10-10	0.26 ± 0.05	0.19 ± 0.05
PEI20-10	0.56 ± 0.05	0.39 ± 0.02
PEI30-10	0.92 ± 0.09	0.60 ± 0.02

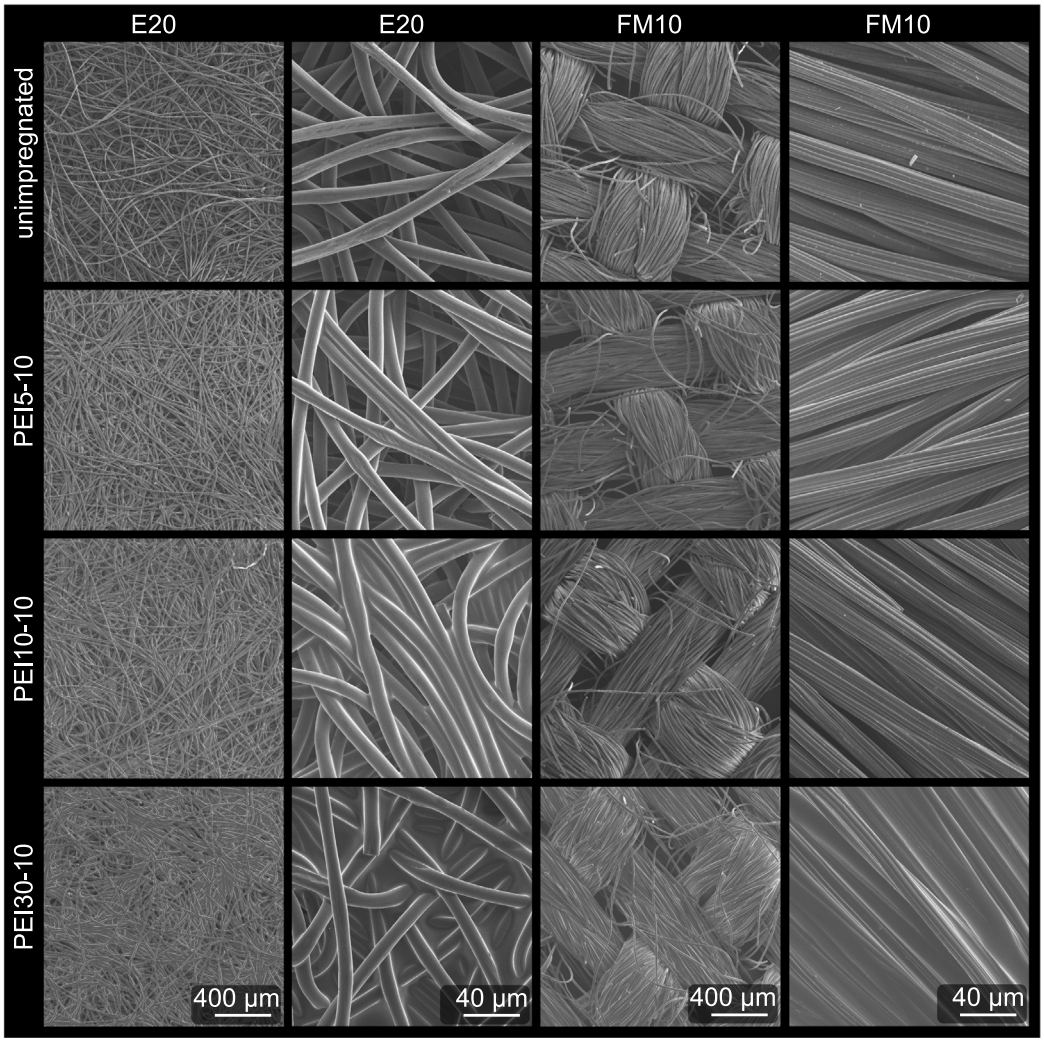


Fig. 4. SEM images of E20 and FM10 before and after PEI impregnation with 5, 10 and 30 wt.% PEI solutions (dwell time 10 s).

controlled conditions, thereby establishing a benchmark of the material properties. Prior to sorption measurements, selective CO_2 uptake was confirmed for all PEI-functionalized E20 samples and for FM10-PEI5-20, FM10-PEI10-10, FM10-PEI20-10, and FM10-PEI30-10, while FM10-PEI5-10 was found to be non-selective due to incomplete surface coverage (see Section 3 in the SI).

3.3.1. CO_2 sorption capacity

Fig. 5 summarizes the CO_2 uptake as a function of PEI loading after 90 min of sorption of 400 ppm CO_2 in argon (Ar) at 30 °C, with Lewatit evaluated as a benchmark under identical conditions. As equilibrium is not reached within 90 min for all samples, this quantity is reported as the 90 min uptake under the specified TGA conditions rather than as an equilibrium capacity.

For both fabrics, the CO_2 capacity increased with increasing PEI loading. At a PEI loading of approximately 0.15 $g_{PEI}\ g_{CF}^{-1}$, similar capacities were obtained for E20 and FM10, whereas at higher loadings E20 consistently achieved higher CO_2 capacities with up to 0.97 mmol g^{-1} at 0.6 $g_{PEI}\ g_{CF}^{-1}$. At PEI loadings exceeding 0.25 $g_{PEI}\ g_{CF}^{-1}$, both fabrics outperformed Lewatit under the applied conditions. Normalized to the amine content, the 90 min uptake corresponds to an amine efficiency of approximately 0.08-0.12 mol CO_2 per mol of nitrogen for both fabrics, decreasing toward the lower end at the thicker PEI coatings.

The monotonic increase in capacity with PEI loading is consistent with the higher density of amine sites. However, equilibrium was not reached within 90 min for E20 and Lewatit, as indicated by continued uptake beyond this timeframe (see Figure S5 in the SI). Comparable

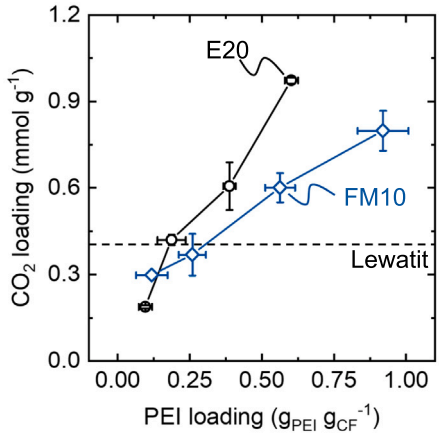


Fig. 5. Thermogravimetric analysis of CO_2 sorption capacity. CO_2 loading of PEI-impregnated E20 and FM10 when exposing all samples to 400 ppm CO_2 in argon at a flow rate of 50 mL min^{-1} at 30 °C for 90 min. The CO_2 loading of Lewatit at the same conditions is shown for benchmark comparison.

non-equilibrium behavior after 90 min has been reported for Lewatit under similar conditions and attributed to combined intrinsic kinetics and internal mass transfer limitations [26].

For the PEI-impregnated fabrics, uptake depends not only on amine content but also on accessibility. Following the framework proposed by Wang et al. [27], PEI-based sorbents can exhibit a distribution of more accessible open regions and transport-restricted closed regions that arise from pore filling and blocked pathways of the substrate. Within this context, the lower capacities observed for FM10 at elevated PEI loadings suggest a larger fraction of transport-restricted polymer domains compared to E20. This interpretation is consistent with the pronounced loss of accessible surface area upon PEI impregnation of FM10 (see Table S1 and Figure S3 in the SI). In contrast, the macroporous structure of E20 appears to maintain higher accessibility of amine sites at high PEI loadings, resulting in higher CO_2 uptake within the applied sorption time. The intrinsic 400 ppm uptake of both fabrics at high PEI loadings is in the range reported for PEI-coated carbon fibers (~1.2 mmol g^{-1} [15]), confirming that the materials are competitive at the sorbent level.

3.3.2. CO_2 sorption and desorption kinetics

Based on the time-dependent uptake and release profiles, sorption and desorption kinetics were evaluated using the Avrami kinetic model [24]. The resulting effective kinetic constants k_a are shown in Fig. 6 and provide a comparative measure of overall sorption and desorption rates as a function of PEI loading.

Across all investigated PEI loadings, FM10 exhibited higher sorption rate constants than E20, indicating faster overall uptake. The highest sorption rate constant of 0.11 min^{-1} was observed for FM10 at 0.12 ± 0.05 $g_{PEI}\,g_{CF}^{-1}$. For both fabrics, sorption rates decreased with increasing PEI loading, consistent with increasing transport and/or kinetic resistances within the thickening polymer phase. At high loadings, the sorption rate constants of E20 approached the value obtained for Lewatit, while FM10 maintained higher rates.

The Avrami model yields a phenomenological rate constant reflecting the combined influence of reaction and diffusion processes. The rate constant k_a therefore enables relative comparison of sorption kinetics, as the Avrami exponent n_a remained similar across all samples (see Table S4 in the SI). However, individual rate-limiting steps cannot be uniquely resolved [24,27–29]. The consistently higher k_a values for FM10 are consistent with its high surface area and microporous texture, which likely promote more distributed polymer deposition and shorter effective diffusion paths. In contrast, the lower surface area of E20 may lead to locally thicker PEI domains and reduced accessibility.

Desorption kinetics follow analogous trends: FM10-based samples exhibited higher desorption rate constants than E20-based materials at comparable PEI loadings, and increasing PEI loading slowed desorption for both substrates. For all samples, 90-100 % of the sorbed CO_2 was released within the first 10 min (see Figure S6 in the SI), indicating reversible uptake under the applied regeneration conditions. Desorption proceeded faster than sorption, which is attributed to the elevated regeneration temperature increasing CO_2 diffusivity and weakening the CO_2-amine interaction.

Taken together, the TGA results reveal a capacity–kinetics tradeoff: while increasing PEI loading enhances intrinsic CO_2 capacity, it simultaneously reduces sorption and desorption rates, with FM10 consistently offering faster kinetics and E20 maintaining higher accessible capacities at elevated loadings. These observations correlate with the fundamental design principle for PEI-based sorbents: A high specific surface area promotes PEI loading and amine site density, but simultaneously leads to pore filling and the formation of thicker polymer domains that restrict internal transport [30]. An ideal substrate would therefore combine a sufficient surface area for a uniformly thin PEI coating with a predominantly macroporous or hierarchically porous architecture that preserves open transport pathways [31]. Thin-film studies of PEI indicate an optimal layer thickness of approximately 50 nm at 400 ppm CO_2, beyond which the accessibility of the amines decreases due to diffusion resistance [20]. In the context of a fabric substrate, this optimum would translate into a high density of thin PEI coatings distributed across a large accessible surface. Such a configuration is more readily achieved on substrates with narrow-fiber architectures and controlled intrafiber and interfiber porosity, such as electrospun nanofiber mats or engineered woven structures with reduced fiber bundle density.

3.4. Influence of PEI loading on dynamic CO_2 sorption and desorption

Dynamic CO_2 sorption and desorption experiments were conducted in a SWM, as described in Section 2.5, to evaluate how PEI loading influences capture behavior under continuous flow conditions. In contrast to the intrinsic sorption behavior obtained from TGA, the experiments presented here reflect the effective performance of the coated sorbent within the structured module, where transport limitations, residence time, and regeneration dynamics determine how much of the intrinsic capacity can be utilized under dynamic operation.

Based on the intrinsic material characterization, the microporous FM10 fabric was selected for dynamic module evaluation in the SWM. Compared to E20, FM10 exhibited consistently faster intrinsic sorption and desorption kinetics across the investigated PEI loadings. Since DAC under continuous flow is often governed by mass-transfer and kinetic limitations rather than equilibrium capacity alone [32], FM10 was therefore selected as the kinetically favorable substrate for the SWM experiments.

Two FM10-based sorbents representing limiting cases identified in the intrinsic characterization were selected for dynamic evaluation: FM10-PEI5-20, exhibiting the fastest intrinsic kinetics, and FM10-PEI30-10, achieving the highest intrinsic CO_2 capacity. These materials correspond to PEI loadings of 0.12 ± 0.05 $g_{PEI}\,g_{CF}^{-1}$ and 0.92 ± 0.09 $g_{PEI}\,g_{CF}^{-1}$, respectively.

Fig. 7 summarizes the dynamic breakthrough and regeneration behavior of both sorbents using 400 ppm CO_2 in N_2 at a flow rate of 100 sccm. During sorption, nearly all CO_2 was captured from the inlet gas stream at the beginning of the experiment for both materials, followed by a gradual CO_2 breakthrough. FM10-PEI5-20 exhibited an earlier breakthrough and a steeper breakthrough front, whereas FM10-PEI30-10 showed delayed breakthrough and a more gradual concentration increase. Within the investigated sorption period, neither sorbent reached full saturation. The maximum dynamic loadings reached 0.05 mmol g^{-1} for FM10-PEI5-20 and 0.3 mmol g^{-1} for FM10-PEI30-10.

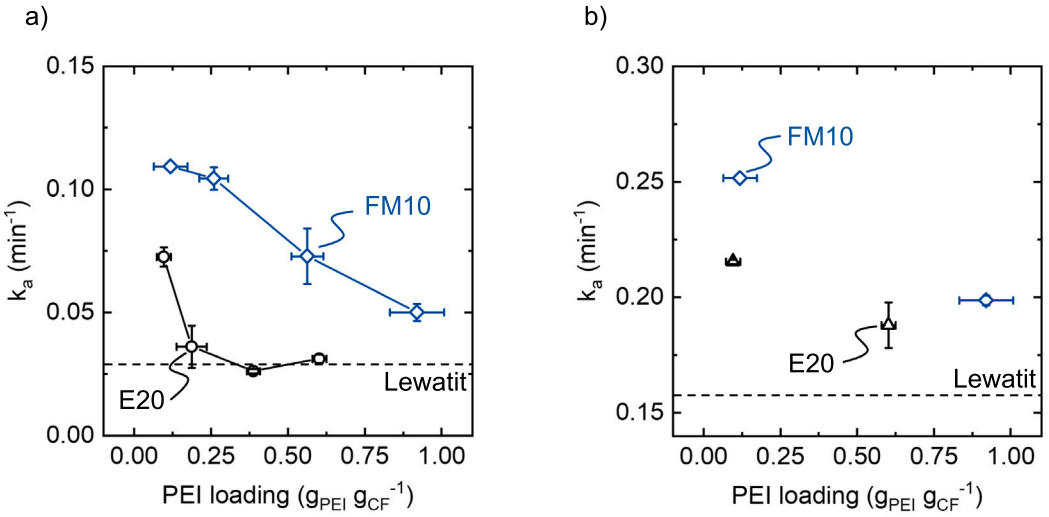


Fig. 6. Kinetic constant k_a of the Avrami kinetic model for (a) CO_2 sorption and (b) desorption of PEI-impregnated E20 and FM10. During sorption, the samples were overflown with 400 ppm CO_2 in argon at a flow rate of 50 mL min^{-1} at 30 °C. A temperature swing to 120 °C was used to initiate the desorption. The Avrami kinetic constant of Lewatit is shown for benchmark comparison.

Following sorption, regeneration was performed by resistively heating the sorbent to approximately 110 °C under N_2 flow. Both sorbents achieved CO_2 regeneration efficiencies of 85-90 %. Due to its higher initial loading, FM10-PEI30-10 achieved a 2.7-fold higher product concentration during desorption compared to FM10-PEI5-20. However, desorption from FM10-PEI30-10 exhibited more pronounced tailing, indicating stronger transport resistance associated with thicker polymer domains.

The sharper breakthrough front observed for FM10-PEI5-20 indicates a narrower mass transfer zone and faster overall uptake under the tested flow conditions, consistent with the higher intrinsic uptake rates observed by TGA. Accordingly, FM10-PEI5-20 achieved a higher dynamic yield of 97 % compared to 95 % for FM10-PEI30-10 until breakthrough, reflecting the more efficient capture of the inlet CO_2 stream at lower PEI loading. In contrast, the delayed breakthrough and higher loading of FM10-PEI30-10 arise from its increased amine density, despite increased transport resistance. These observations demonstrate that the intrinsic capacity–kinetics trade-off identified as material property translates qualitatively to dynamic module operation.

Sorption was continued until the outlet concentration reached at least 300 ppm and was then switched to regeneration before complete saturation. At this stage of the breakthrough curve, the incremental uptake rate is already low, such that accessing the remaining intrinsic capacity would require disproportionately longer sorption times. Comparison with TGA shows that 15-30 % of the intrinsic capacity was utilized within the investigated sorption time under dynamic operation. This utilization gap reflects the combined influence of finite residence time and non-equilibrium uptake under flow, including external gas–solid mass transfer and transport/kinetic resistances within the PEI phase.

The elevated desorption peak concentration observed for FM10-PEI30-10 indicates a higher attainable product concentration during regeneration, albeit with more pronounced desorption tailing reflecting stronger transport resistance within thicker PEI domains. This illustrates a trade-off between achievable product concentration and desorption rate under dynamic operation.

To translate these dynamic differences into a process-relevant metric, we evaluated a simplified, illustrative cyclic operating scenario linking the achievable CO_2 uptake to the required cycle time. Sorption, desorption, and cooling were cycled continuously, assuming sorption to a fixed utilization of $x = q_{BTC}/q_{TGA} = 0.1$, regeneration of 80 % of the sorbed CO_2, and cooling to 40 °C after each regeneration. The difference between the sorption and desorption loadings defines the working capacity per cycle. These assumptions are illustrative rather than optimized and serve to compare the two sorbents on a common, time-resolved basis. Under them, FM10-PEI5-20 reached a working capacity of 0.044 mmol g^{-1} per cycle within a cycle time of approximately 3 h, whereas FM10-PEI30-10 reached a higher working capacity of 0.099 mmol g^{-1} per cycle within a longer cycle time of approximately 6.5 h.

Fig. 7d shows the resulting cumulative CO_2 capture. FM10-PEI30-10 captured more CO_2 cumulatively than FM10-PEI5-20 despite its substantially longer cycle time. On a mass-specific basis, however, the two sorbents are nearly equivalent, with a mass productivity of 0.015 mmol g^{-1} h^{-1} for both, because the higher per-cycle capacity of FM10-PEI30-10 is offset by its longer cycle time. The advantage of the higher-loading sorbent therefore emerges at the module level. Referenced to the internal module volume, the volumetric productivity is 3.5 mmol L^{-1} h^{-1} for FM10-PEI30-10 and 2.0 mmol L^{-1} h^{-1} for FM10-PEI5-20, since the higher PEI loading packs more working capacity into the fixed module volume. The relative ranking of the two sorbents thus depends on the chosen metric: dynamic yield favors the low-loading sorbent, whereas product concentration and volumetric productivity favor the high-loading one.

3.5. Influence of operating conditions on dynamic CO_2 sorption and desorption

3.5.1. Gas flow rate

Fig. 8 compares the dynamic CO_2 sorption and desorption behavior of FM10-PEI30-10 at gas flow rates of 50 sccm and 100 sccm. The experiment at 100 sccm, discussed in the preceding section, serves as the reference condition.

At the lower flow rate of 50 sccm, sorption exhibited delayed breakthrough and a wider mass transfer zone compared to 100 sccm. Correspondingly, the CO_2 loading increased more gradually over time, as shown in Fig. 8d. During regeneration, comparable product concentrations were obtained at both flow rates, while the desorption profile at 50 sccm showed more pronounced tailing. The pressure drop across the module remained small, increasing from about 45 mbar at 50 sccm to about 80 mbar at 100 sccm.

Reducing the gas flow rate increases the residence time of the gas within the module and thereby enhances the contact time between the gas phase and the sorbent. To quantify the relation of convective to

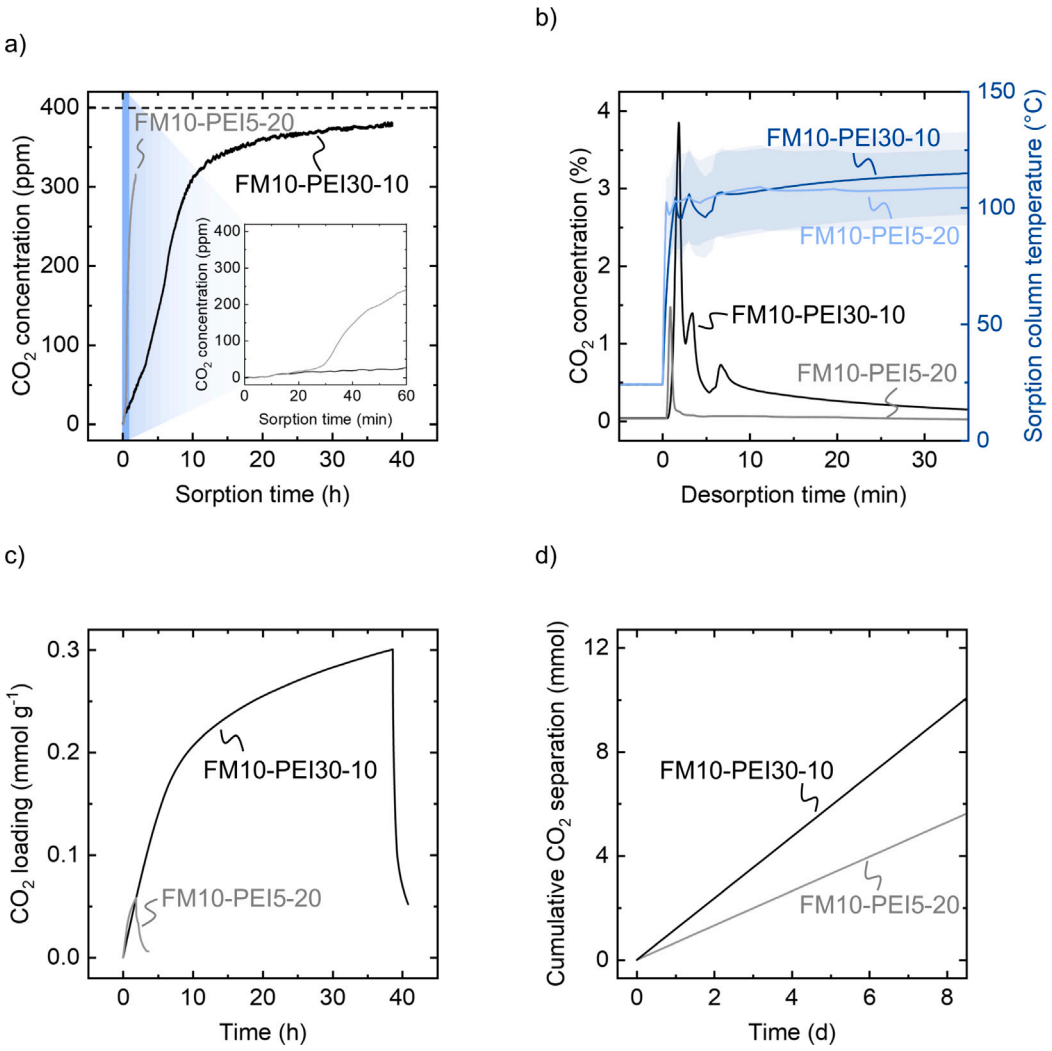


Fig. 7. Dynamic CO_2 sorption and regeneration of FM10 impregnated with 5 wt.% and 30 wt.% PEI, corresponding to PEI loadings of 0.12 ± 0.05 $g_{PEI}\,g_{CF}^{-1}$ (FM10-PEI5-20) and 0.92 ± 0.09 $g_{PEI}\,g_{CF}^{-1}$ (FM10-PEI30-10), respectively. (a) CO_2 outlet concentration during sorption using 400 ppm CO_2 in N_2 at a flow rate of 100 sccm. (b) CO_2 outlet concentration and module temperature during desorption by resistive heating. (c) CO_2 loading of the sorbent during sorption and desorption. (d) Cumulative CO_2 captured over time under a simplified cyclic operating scenario (sorption to $q_{BTC}/q_{TGA} = 0.1$, 80 % regeneration, cooling to 40 °C).

diffusive transport, the dimensionless Péclet number (Pe), defined here as the ratio of convective to diffusive axial transport, $Pe = uL/D_{ax}$, where u is the superficial velocity, L the module length, and D_{ax} the axial diffusion coefficient of CO_2 in N_2, is used. Flow rates of 50 sccm and 100 sccm correspond to Pe values of approximately 22 and 44, respectively, based on a CO_2 diffusion coefficient in air of approximately 1.5×10^{-5} $m^2\,s^{-1}$ [33]. Both values indicate convection-dominated axial transport, yet the lower Pe at 50 sccm reflects a greater relative contribution of diffusive transport, allowing more time for CO_2 to be transferred from the bulk gas phase into the pore network and the PEI phase. Consequently, a higher dynamic loading is observed for the same cumulative inlet CO_2 exposure, as shown in Fig. 8c.

When evaluated with respect to the same cumulative processed CO_2 volume, the experiment at 50 sccm achieves a higher CO_2 uptake than the 100 sccm reference, indicating an increased dynamic yield. However, this improvement occurs at the expense of productivity. The comparison of both flow rates therefore illustrates the trade-off between yield and productivity, highlighting the strong influence of gas flow rate on capture performance under DAC-relevant conditions. Capturing the same cumulative CO_2 at 50 sccm requires approximately 15 h of sorption, because the lower flow rate processes proportionally less gas per unit time despite the higher per-gram dynamic loading; the mass productivity is therefore lower at 50 sccm while the dynamic yield is higher, quantifying the trade-off illustrated in Fig. 8c and d.

3.5.2. Humidity

Fig. 9 compares the dynamic CO_2 sorption and regeneration behavior of FM10-PEI30-10 under dry and humid conditions at a gas flow rate of 50 sccm. Under humid operation, no CO_2 breakthrough was observed within the investigated sorption period, whereas gradual breakthrough occurred under dry conditions. The correspondingly higher CO_2 loading under humid conditions is shown in Fig. 9c. During regeneration, humid operation produced lower peak CO_2 concentrations than dry conditions despite the higher sorption loading. In addition, the temperature rise during regeneration was delayed under humid conditions, as reflected by the temperature profiles in Fig. 9b.

The suppressed breakthrough under humid conditions indicates faster overall CO_2 uptake, commonly attributed to swelling of the PEI phase in the presence of water, which increases polymer chain mobility and reduces transport resistance within the polymer matrix [22]. Swelling thereby enhances amine accessibility and facilitates CO_2 transport. In terms of dynamic yield, humid operation outperformed dry conditions.

The lower product concentration observed under humid conditions is consistent with stronger CO_2 binding in the presence of water, in line

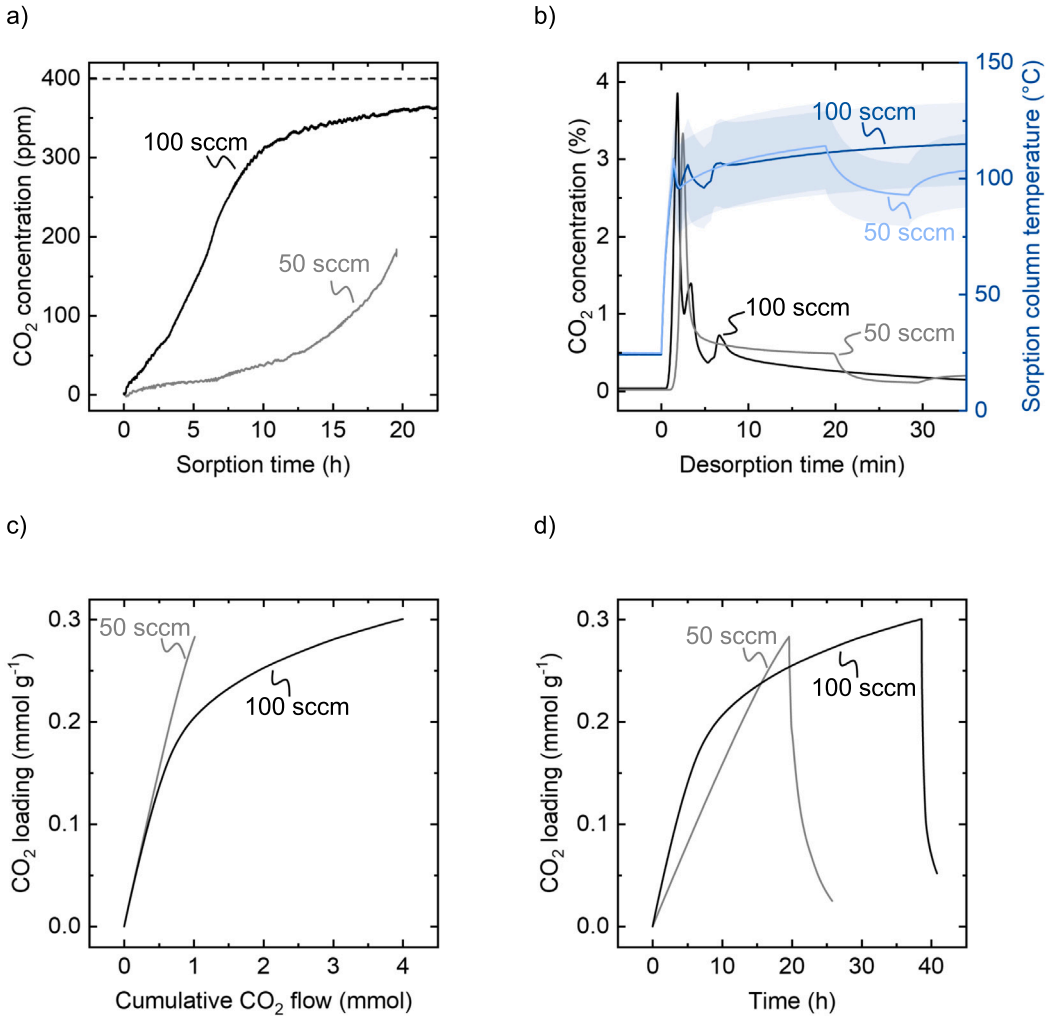


Fig. 8. Dynamic CO_2 sorption and regeneration of FM10-PEI30-10 ($0.92 \pm 0.09\,g_{PEI}\,g_{CF}^{-1}$) at gas flow rates of 50 and 100 sccm. (a) CO_2 outlet concentration during sorption using 400 ppm CO_2 in N_2 at room temperature. (b) CO_2 outlet concentration and module temperature during regeneration under N_2 flow with resistive heating. Temperature variations correlate to manual temperature control by resistive heating. (c) CO_2 loading of the sorbent as a function of cumulative inlet CO_2 during sorption. (d) CO_2 loading of the sorbent during sorption and desorption.

with humid amine sorption mechanisms reported in the literature [31, 34]. At later stages of desorption, the increased mobility of CO_2 within the swollen polymer phase promotes continued release, enabling high regeneration degrees despite the slower desorption response, as shown in Fig. 9d. Simultaneously, co-adsorbed water increases the effective heat capacity of the sorbent, contributing to the delayed temperature rise and higher energy demand during the initial phase of regeneration (see Figure S8 in the SI).

Taken together, humid operation increases dynamic yield but reduces product concentration. Co-adsorbed water raises the energy demand in the early stage of regeneration, up to a regeneration degree of about 87 %. The total electrical energy required to reach complete regeneration was nonetheless lower under humid than under dry conditions, 158 kJ against 317 kJ. Combined with the higher CO_2 loading captured under humid operation, this corresponds to an approximately 2.2-fold lower specific regeneration energy. Humidity therefore acts as an additional operating lever alongside flow rate for the operational optimization of electrified DAC.

To place these values in context, the measured regeneration energy in Fig. 9d was decomposed into its physical contributions, as detailed in Table S5 in the SI. Normalized to the mass of CO_2 desorbed, the input corresponds to specific regeneration energies of approximately $8.6 \times 10^3\,GJ\,t^{-1}$ under humid and $1.9 \times 10^4\,GJ\,t^{-1}$ under dry conditions. These values lie far above the thermodynamic minimum and above conventional DAC estimates of a few $GJ\,t^{-1}$ [6], because the energy is overwhelmingly parasitic. Intrinsic CO_2 and water desorption together account for less than 0.5 % of the input. Sensible heating of the sorbent and the surrounding steel housing contributes about 16 % under humid and about 8 % under dry conditions, and heat loss to the surroundings accounts for the remainder. The regeneration energy of this laboratory module is therefore set by heat losses rather than by the sorbent, since a steel housing of 550 g surrounds only about 3 g of sorbent. The lower total energy under humid conditions reflects the shorter high-temperature hold needed to complete regeneration. It nonetheless identifies module heat management, not the sorbent, as the dominant energy lever. As the absolute values are loss-dominated and were obtained under manual temperature control, we treat the humid and dry crossover as a module-level observation rather than an intrinsic property. For context, optimized Joule-heated DAC contactors have been reported at specific regeneration energies of 3.5-3.7 $GJ\,t^{-1}$ [35] and conventional temperature swing adsorption (TSA)/VTSA systems at 5.1-8.4 $GJ\,t^{-1}$ [6]; the gap to the present values reflects the unoptimized module form factor rather than any fundamental limitation of resistive regeneration.

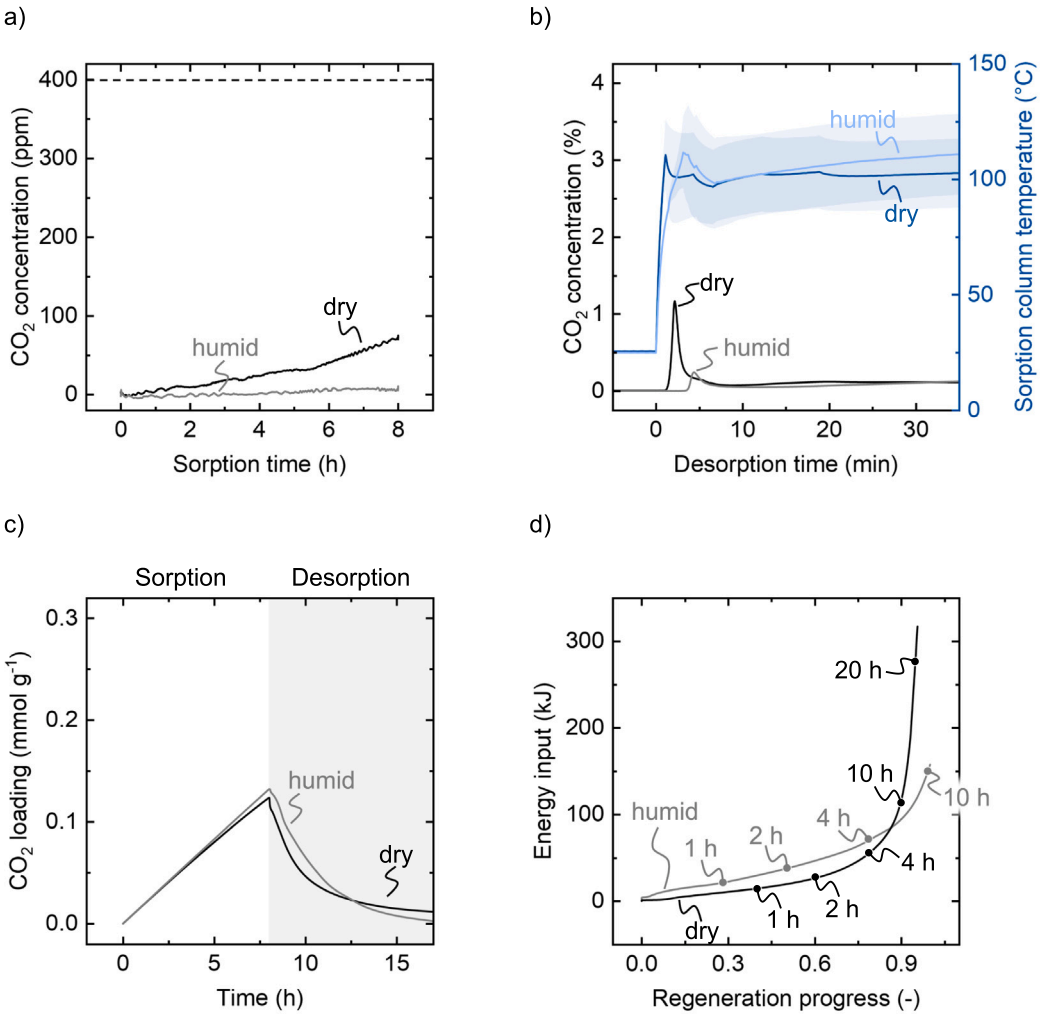


Fig. 9. Dynamic CO_2 sorption and regeneration of FM10-PEI30-10 ($0.92 \pm 0.09\ g_{PEI}\ g_{CF}^{-1}$) under dry and humid conditions. (a) CO_2 outlet concentration during sorption using 400 ppm CO_2 in N_2 at a flow rate of 50 sccm. The inlet H_2O concentration was 2.67 vol.% during humidified sorption. (b) CO_2 outlet concentration and module temperature during regeneration under N_2 flow with resistive heating. (c) CO_2 loading of the sorbent during sorption and desorption. (d) Cumulative energy input as a function of regeneration progress during desorption.

3.6. Cyclic stability of dynamic CO_2 sorption and desorption

To assess the stability of the module sorbent under repeated operation, FM10-PEI30-10 was cycled four times between dry sorption and resistive regeneration, as shown in Fig. 10. The working capacity per cycle decreased moderately from 0.116 mmol g^{-1} in the first cycle to 0.095 mmol g^{-1} in the fourth, corresponding to a retention of about 82 %. Over the same cycles, the regenerability decreased from 92 % to 81 %.

The gradual decline may reflect incomplete regeneration within the fixed desorption window or partial loss of accessible amine sites through degradation under repeated thermal cycling [25]. The retained working capacity nonetheless indicates that the sorbent stays functional over the investigated cycles under resistive regeneration. These four dry cycles provide an initial stability assessment. Cyclic operation under humidity and over longer cycle numbers is addressed as a direction for future work. The moderate capacity decline observed here is consistent with the small losses reported by Lee et al. over ten dry resistive cycles at 110 °C [15], and with the broader observation that PEI-based sorbents typically lose a fraction of their initial capacity before stabilizing over 20–30 cycles, suggesting that the four-cycle decline reported here may not be representative of the long-term steady-state performance.

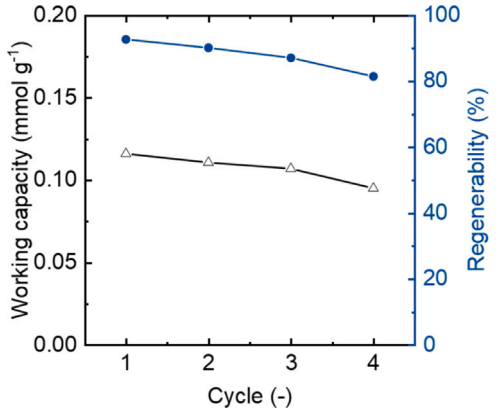


Fig. 10. Cyclic CO_2 working capacity and regenerability of FM10-PEI30-10 ($0.92 \pm 0.09\ g_{PEI}\ g_{CF}^{-1}$). Sorption was conducted for 8 h at ambient temperature with 100 sccm of dry 400 ppm CO_2 in N_2. Desorption was conducted for 4 h with 100 sccm N_2 at 120 °C.

4. Conclusion

This work investigated PEI-impregnated carbon fabrics as electrically heatable, structured sorbents for DAC, with emphasis on how substrate structure, coating architecture, and operating conditions jointly determine capture performance under continuous flow and electrothermal regeneration.

Both carbon fabrics provided electrically suitable supports for resistive regeneration. Intrinsic material characterization revealed a clear trade-off between sorption capacity and kinetics. Increasing PEI loading increased intrinsic CO_2 capacity (up to $0.97\,mmol\,g^{-1}$ for E20) but slowed sorption and desorption, indicating increasing transport and/or kinetic resistances within the thickening polymer phase. At comparable PEI loading, FM10 showed consistently faster intrinsic uptake and release kinetics, whereas E20 maintained higher accessible capacities at high loadings within the applied sorption time, reflecting differences in polymer distribution and accessibility imposed by the substrate pore structure.

These results demonstrate that increasing surface area and polymer loading alone does not necessarily maximize usable sorbent performance. Instead, substrate architecture influences the balance between amine density and transport accessibility, which determines the fraction of the intrinsic capacity that remains available under realistic operating conditions. Revisiting the hypothesis of our prior work, thin and accessible PEI coatings remain necessary but are not sufficient on their own: even the kinetically favorable FM10 utilized only 15-30 % of its intrinsic capacity in the module, so closing the intrinsic-to-dynamic gap depends as much on module design and operation as on the coating.

When deployed in the resistively heated SWM under dynamic flow, these intrinsic trends translated qualitatively to dynamic operation in the SWM, but only a fraction of the intrinsic capacity was utilized within the applied sorption window. Lower PEI loadings produced steeper breakthrough fronts and higher dynamic yield, whereas higher PEI loadings increased dynamic CO_2 loading and enabled higher attainable product concentrations during regeneration, albeit with more pronounced desorption tailing.

The intrinsic-to-dynamic utilization gap was strongly affected by operating conditions. Reducing the gas flow rate increased residence time and improved dynamic yield at the expense of productivity. Humidity accelerated uptake and increased dynamic loading through enhanced mobility and accessibility of the hydrated PEI phase, while simultaneously affecting regeneration behavior through co-adsorbed water and reduced product concentration. These results highlight that operating conditions provide an additional design lever beyond sorbent formulation.

Overall, the results demonstrate that the usable performance of electrified TSA for DAC is governed by the coupled design of substrate morphology, PEI loading, contactor architecture, and operating strategy rather than by intrinsic material properties alone.

At the module level, these findings identify two primary routes for improving electrified DAC performance. First, regeneration energy was dominated by parasitic heat losses rather than by sorbent regeneration itself, making thermal management and reduction of the housing-to-sorbent ratio the dominant energy optimization strategies. Second, only 15-30 % of the intrinsic sorbent capacity was accessed during dynamic operation, indicating that improving gas–sorbent contact and transport pathways is essential. Increasing sorbent loading can improve volumetric productivity, but does not necessarily improve mass-specific productivity because higher capacity is accompanied by slower kinetics. Therefore, future module optimization should prioritize dynamic utilization of the sorbent capacity rather than maximizing intrinsic uptake alone.

Future work should therefore focus on process-informed optimization, including (i) exploring substrate architectures, such as nanofiber mats or woven structures with reduced fiber bundle density, that promote uniformly thin PEI coatings and thereby reduce the capacity–kinetics trade-off identified here, (ii) tailoring PEI distribution within existing substrates (e.g., graded loadings) to reduce late-stage transport limitations, (iii) quantifying mass-transfer contributions (gas–solid vs. polymer-phase) through targeted variation of hydrodynamics and structured geometry, (iv) extending cyclic testing under controlled humidity to resolve productivity–yield–product concentration trade-offs and regeneration energy demand, and (v) assessing long-term stability under relevant operating conditions.

CRediT authorship contribution statement

Carla Esch: Writing – review & editing, Writing – original draft, Visualization, Validation, Supervision, Project administration, Methodology, Investigation, Funding acquisition, Formal analysis, Data curation, Conceptualization. **Jacqueline Kieven:** Visualization, Investigation, Data curation. **Antonia Geiser:** Visualization, Investigation, Data curation. **Roman Ryapushkin:** Software. **Wibke Zängler:** Writing – review & editing, Conceptualization. **Matthias Wessling:** Writing – review & editing, Supervision, Resources, Project administration, Methodology, Funding acquisition, Conceptualization.

Declaration of Generative AI and AI-assisted technologies in the writing process

During the preparation of this work, ChatGPT and Claude were used to refine writing and enhance readability. The authors thoroughly reviewed and edited the AI-generated content as necessary, and take full responsibility for the content of this publication.

Declaration of competing interest

The authors declare that they have no known competing financial interests or personal relationships that could have appeared to influence the work reported in this paper.

Acknowledgments

The authors thank Karin Faesen for the high-quality SEM images. This work was supported by the German Federal Ministry of Education and Research (BMBF) under the project “DryHy” (FKZ 03SF0716B). M.W. acknowledges the DFG funding through the Gottfried Wilhelm Leibniz Award 2019 (WE 4678/12-1). M.W. appreciates the support from the Alexander-von-Humboldt foundation.

Appendix A. Supplementary data

Supplementary material related to this article can be found online at https://doi.org/10.1016/j.cej.2026.179238.

Data availability

Data will be made available on request.

References

[1] M. Erans, E.S. Sanz-Pérez, D.P. Hanak, Z. Clulow, D.M. Reiner, G.A. Mutch, Direct air capture: Process technology, techno-economic and socio-political challenges, Energy & Environ. Sci. 15 (4) (2022) 1360–1405, http://dx.doi.org/10.1039/D1EE03523A.

[2] R.Q. Wang, L. Jiang, Y.D. Wang, A.P. Roskilly, Energy saving technologies and mass-thermal network optimization for decarbonized iron and steel industry: A review, J. Clean. Prod. 274 (2020) 122997, http://dx.doi.org/10.1016/j.jclepro.2020.122997.

[3] D.W. Keith, G. Holmes, D. St. Angelo, K. Heidel, A process for Capturing CO_2 from the atmosphere, Joule 2 (8) (2018) 1573–1594, http://dx.doi.org/10.1016/j.joule.2018.05.006.

[4] I. Filahi, A.H. Assen, Y. Belmabkhout, J. Chaouki, Passive adsorptive direct air capture (PADAC) using a nature-assisted temperature swing process: A sustainable solution for residential CO_2 emissions, Energy Convers. Manage. 338 (2025) 119925, http://dx.doi.org/10.1016/j.enconman.2025.119925.

[5] M. van der Spek, A. Bardow, C. M. Baum, V. Bolongaro, V. Dufour-Décieux, C. Esch, L. Fritz, S. Garcia, C. Hamann, D. Hondeborg, A. Kiani, S. Lueck, S. Kalpeshkumar Patel, S. Bo Peh, M. Pisciotta, P. Psarras, T. Repke, P. Alejandra Sáenz-Cavazos, I. Schulte, D. Shu, Q. Shu, B. Sovacool, J. Strefler, S. Vallejo Castaño, J.-Y. Wang, M. Wessling, J. Wilcox, J. Young, J. C. Minx, An ecosystem of carbon dioxide removal reviews – Part 1: Direct air CO_2 capture and storage, Energy & Environ. Sci. (2025) http://dx.doi.org/10.1039/D5EE01732G.

[6] S. Deutz, A. Bardow, Life-cycle assessment of an industrial direct air capture process based on temperature–Vacuum swing adsorption, Nat. Energy 6 (2) (2021) 203–213, http://dx.doi.org/10.1038/s41560-020-00771-9.

[7] V. Stampi-Bombelli, M. van der Spek, M. Mazzotti, Analysis of direct capture of CO_2 from ambient air via steam-assisted temperature–Vacuum swing adsorption, Adsorption 26 (7) (2020) 1183–1197, http://dx.doi.org/10.1007/s10450-020-00249-w.

[8] B. Verougstraete, M. Gholami, Y. Gomez-Rueda, E. Pérez-Botella, M. Schoukens, T.R.C. Van Assche, J.F.M. Denayer, Advancements and challenges in electric heating for enhanced temperature swing adsorption processes, Sep. Purif. Technol. 353 (2024) 128522, http://dx.doi.org/10.1016/j.seppur.2024.128522.

[9] C.A. Grande, A.E. Rodrigues, Electric swing adsorption for CO_2 removal from flue gases, Int. J. Greenh. Gas Control. 2 (2) (2008) 194–202, http://dx.doi.org/10.1016/S1750-5836(07)00116-8.

[10] T.S. Lee, J.H. Cho, S.H. Chi, Carbon dioxide removal using carbon monolith as electric swing adsorption to improve indoor air quality, Build. Environ. 92 (2015) 209–221, http://dx.doi.org/10.1016/j.buildenv.2015.04.028.

[11] Q. Zhao, F. Wu, Y. He, P. Xiao, P.A. Webley, Impact of operating parameters on CO_2 capture using carbon monolith by electrical swing adsorption technology (ESA), Chem. Eng. J. 327 (2017) 441–453, http://dx.doi.org/10.1016/j.cej.2017.06.123.

[12] R.P.P.L. Ribeiro, C.A. Grande, A.E. Rodrigues, Activated carbon honeycomb monolith – Zeolite 13X hybrid system to capture CO_2 from flue gases employing electric swing adsorption, Chem. Eng. Sci. 104 (2013) 304–318, http://dx.doi.org/10.1016/j.ces.2013.09.011.

[13] A. Masala, J.G. Vitillo, G. Mondino, G. Martra, R. Blom, C.A. Grande, S. Bordiga, Conductive ZSM-5-Based Adsorbent for CO_2 Capture: Active phase vs monolith, Ind. Eng. Chem. Res. 56 (30) (2017) 8485–8498, http://dx.doi.org/10.1021/acs.iecr.7b01058.

[14] Q. Zhao, F. Wu, Y. Men, X. Fang, J. Zhao, P. Xiao, P.A. Webley, C.A. Grande, CO_2 capture using a novel hybrid monolith (H-ZSM5/Activated carbon) as adsorbent by combined vacuum and electric swing adsorption (VESA), Chem. Eng. J. 358 (2019) 707–717, http://dx.doi.org/10.1016/j.cej.2018.09.196.

[15] W.H. Lee, X. Zhang, S. Banerjee, C.W. Jones, M.J. Realff, R.P. Lively, Sorbent-coated carbon fibers for direct air capture using electrically driven temperature swing adsorption, Joule 7 (6) (2023) 1241–1259, http://dx.doi.org/10.1016/j.joule.2023.05.016.

[16] H. Li, M.E. Zick, T. Trisukhon, M. Signorile, X. Liu, H. Eastmond, S. Sharma, T.L. Spreng, J. Taylor, J.W. Gittins, C. Farrow, S.A. Lim, V. Crocellà, P.J. Milner, A.C. Forse, Capturing carbon dioxide from air with charged-sorbents, Nature 630 (8017) (2024) 654–659, http://dx.doi.org/10.1038/s41586-024-07449-2.

[17] C. Esch, M. Mehltretter, J. Neese, S. Herrmann, R. Ryapushkin, C.J. Linnartz, M. Wessling, Resistively heated spiral wound module for temperature swing adsorption of CO_2, Chem. Eng. J. 524 (2025) 168727, http://dx.doi.org/10.1016/j.cej.2025.168727.

[18] K. Xuan, L. Zhong, R.M. Othman, G.P. Lithoxoos, F. Almansour, A.N. Shakhs, Y. Liu, X. Zhu, N. Duan, X. Sun, W.-P. Pan, On CO_2 capture capacity and mechanisms for zeolite templated carbon, MOF-199, and 13X zeolite in dry and humid conditions, Sep. Purif. Technol. 363 (2025) 132080, http://dx.doi.org/10.1016/j.seppur.2025.132080.

[19] S.-T. Yang, J.-Y. Kim, J. Kim, W.-S. Ahn, CO_2 capture over amine-functionalized MCM-22, MCM-36 and ITQ-2, Fuel 97 (2012) 435–442, http://dx.doi.org/10.1016/j.fuel.2012.03.034.

[20] J.R. Hoffman, A.E. Baumann, C.M. Stafford, Thickness dependent CO_2 adsorption of poly(Ethyleneimine) thin films for direct air capture, Chem. Eng. J. 481 (2024) 148381, http://dx.doi.org/10.1016/j.cej.2023.148381.

[21] P. Sharma, S. Chakrabarty, S. Roy, R. Kumar, Molecular view of CO_2 Capture by polyethylenimine: Role of structural and dynamical heterogeneity, Langmuir 34 (17) (2018) 5138–5148, http://dx.doi.org/10.1021/acs.langmuir.8b00204.

[22] J.R. Hoffman, A.E. Baumann, C.M. Stafford, The role of humidity in enhancing CO_2 capture efficiency in poly(Ethyleneimine) thin films, Chem. Eng. J. 507 (2025) 160347, http://dx.doi.org/10.1016/j.cej.2025.160347.

[23] S. Wang, Z. Wang, Y. Huang, S. Deng, M. Lin, Optimizing hydroxide-functionalized carbon dioxide adsorbents: impact of pore structure on adsorption performance, Energy Proc. (2025).

[24] M. Avrami, Kinetics of phase change. Part I. General theory, J. Chem. Phys. 7 (12) (1939) 1103–1112, http://dx.doi.org/10.1063/1.1750380.

[25] A. Heydari-Gorji, A. Sayari, Thermal, oxidative, and CO2-induced degradation of supported polyethylenimine adsorbents, Ind. Eng. Chem. Res. 51 (19) (2012-05-16) 6887–6894, http://dx.doi.org/10.1021/ie3003446.

[26] B. Balasubramaniam, E. Forbes, C. Picard, J.A. Sawada, A. Rajendran, Equilibrium and kinetic studies of unary CO_2 and H_2O adsorption on lewatit VP OC 1065 for direct air capture of co_2, 2025, http://dx.doi.org/10.26434/chemrxiv-2025-mpk7x.

[27] S. Wang, M. Xie, S. Wang, Y. Zhuo, Kinetic model describing the effect of amine loading and temperature on CO_2 capture by solid amine adsorbent, Carbon Capture Sci. Technol. 17 (2025) 100491, http://dx.doi.org/10.1016/j.ccst.2025.100491.

[28] B. Ohs, M. Krödel, M. Wessling, Adsorption of carbon dioxide on solid amine-functionalized sorbents: A dual kinetic model, Sep. Purif. Technol. 204 (2018) 13–20, http://dx.doi.org/10.1016/j.seppur.2018.04.009.

[29] P. Bollini, N.A. Brunelli, S.A. Didas, C.W. Jones, Dynamics of CO_2 Adsorption on amine adsorbents. 1. Impact of heat effects, Ind. Eng. Chem. Res. 51 (46) (2012) 15145–15152, http://dx.doi.org/10.1021/ie301790a.

[30] A. Holewinski, M.A. Sakwa-Novak, C.W. Jones, Linking CO2 sorption performance to polymer morphology in aminopolymer/silica composites through neutron scattering, J. Am. Chem. Soc. 137 (36) (2015) 11749–11759.

[31] G. Rim, P. Priyadarshini, M. Song, Y. Wang, A. Bai, M.J. Realff, R.P. Lively, C.W. Jones, Support pore structure and composition strongly influence the direct air capture of CO_2 on supported amines, J. Am. Chem. Soc. 145 (13) (2023) 7190–7204, http://dx.doi.org/10.1021/jacs.2c12707.

[32] J. Young, F. Mcilwaine, B. Smit, S. Garcia, M. van der Spek, Process-informed adsorbent design guidelines for direct air capture, Chem. Eng. J. 456 (2023) 141035, http://dx.doi.org/10.1016/j.cej.2022.141035.

[33] A. Lannus, E.D. Grossmann, Modified ney-armistead cell for gas diffusion measurements, Ind. Eng. Chem. Fundam. 9 (4) (1970) 655–657.

[34] R.L. Siegelman, P.J. Milner, A.C. Forse, J.-H. Lee, K.A. Colwell, J.B. Neaton, J.A. Reimer, S.C. Weston, J.R. Long, Water enables efficient CO_2 capture from natural gas flue emissions in an oxidation-resistant diamine-appended metal–organic framework, J. Am. Chem. Soc. 141 (33) (2019) 13171–13186, http://dx.doi.org/10.1021/jacs.9b05567.

[35] S. Zhao, Y. Zhang, Y. Ning, L. Li, J. Lu, X. Wang, F. Wang, Z. Wei, Z. Huang, H. Lin, Electrically conductive amine-functionalized adsorbents driven by joule heating for direct air capture, ACS Sustain. Chem. Eng. 13 (36) (2025) 14949–14960, http://dx.doi.org/10.1021/acssuschemeng.5c05203.